Molecular Crystals and Liquid Crystals Incorporating Nonlinear Optics

Publication details, including instructions for authors and subscription information:
http://www.tandfonline.com/loi/gmcl17

Thermal and Mechanical Instabilities in Nonaqueous Lamellar Lyotropic Lecithin-Ethylenglycol

A. G. Petro [a b], M. Cagnon [a], Y. Galerne [a] & G. Durand [a]

[a] Laboratoire de Physique des Solides, Université de Paris-Sud, 91 405, Orsay, Cedex France

[b] Institute of Solid State Physics, Bulgarian Academy of Sciences, SOFIA, 1184, 72 Lenin Blvd., Bulgaria

Version of record first published: 19 Dec 2006.

To cite this article: A. G. Petro , M. Cagnon , Y. Galerne & G. Durand (1988): Thermal and Mechanical Instabilities in Nonaqueous Lamellar Lyotropic Lecithin-Ethylenglycol, Molecular Crystals and Liquid Crystals Incorporating Nonlinear Optics, 154:1, 179-193

To link to this article: http://dx.doi.org/10.1080/00268948808078731

Mol. Cryst. Liq. Cryst., 1988, Vol. 154, pp. 179–193
Photocopying permitted by license only

Printed in the United States of America

Thermal and Mechanical Instabilities in Nonaqueous Lamellar Lyotropic Lecithin-Ethylenglycol

A. G. PETROV,† M. CAGNON, Y. GALERNE and G. DURAND

Laboratoire de Physique des Solides, Université de Paris-Sud, 91 405 Orsay Cedex (France)

(*Received April 10, 1987*)

A method for preparation of homeotropic monodomains of the lamellar lyomesophase of synthetic DL-β − γ-dilauroyl-α-lecithin plus ethylenglycol is developed. It implied a slow growth of monodomains from the isotropic melt, between two silane-fueated glass plates. Compression and curvature elastic constants of such monodomains are measured from the observation of thermally and mechanically induced undulation instabilities. The penetration length, measured by quasielastic Rayleigh scattering of light, compares with the layer thickness measured by X-rays. This lyomesophase provides a good example of a room temperature smectic-A like liquid crystal with a very broad range of thermal stability.

MATERIALS AND METHODS

Nonaqueous lyomesophases of lecithin where water is replaced by ethylenglycol were proposed by Friberg.[1] Such systems offer important experimental advantages compared to the aqueous ones, because ethylenglycol is less volatile than water (b.p. 197°C) and it keeps more easily its initial concentration during the experiments. Additionally, dilauroyl lecithin mesophases have the advantage of being in the L_α-state at room temperature. Synthetic dilauroyl lecithin (DLL) (rac.-1,2 Dilauroyl glycero-3-phosphorylcholin, (Fluka)) and ethylenglycol (EG) (Fluka Garantie) are used. Weighted amounts of DLL and EG are mixed in Pyrex glass tubes. The EG concentration is kept

†Permanent address: Institute of Solid State Physics, Bulgarian Academy of Sciences, SOFIA 1184, 72 Lenin Blvd., Bulgaria.

at 35% wf. With the molecular weights (M_{DLL} = 621.84 M_{EG} = 62.07) this gives a molar ratio EG/DLL = 5.4/1. To achieve better mixing and to get a mesophase free of air bubbles it is necessary to heat the mixture up to 130°C for a short time (30 sec) followed by a centrifugation on a Beckman-ultracentrifuge at 10000 rpm and 40°C rotor temperature for 10 min. Eventually, this procedure should be repeated 2 or 3 times. During the heating of the closed glass tube some amount of EG is evaporated and condensed on the tube walls, but after centrifugation these tiny EG drops go back to the mixture. Weighting of the sample after the accomplishment of the mixing procedure confirmed that only 0.1% of the total weight of the mixture was lost.

To produce homeotropic monodomains we use, like Powers and Clark,[2] silane-treated plates (DC XZ 22300 silane experimental sample, provided by N. V. Dow Corning, S. A., Belgium), applying the silane coating from water solution (0.1% wt) and incubating the treated plates at 100°C in dry nitrogen atmosphere for 1 h. However, the method in Ref. 2, developed for aqueous samples with very low water content (2–10% wt) does not work in our case. Prolonged keeping of the sample below its transition temperature to isotropic phase (125°C) does not produce any changes in its initial, randomly coloured texture, which for sample thicknesses more than 100 μm was mostly planar. So, we had to modify the method.

A drop of the highly viscous at room temperature lyomesophase is applied over one of the silane-treated glass plates with a Mylar spacer in the form of a square frame over it and then pressed by the second plate to spread as a circular drop, preferably without touching the frame of the spacer. Reasonable hermetization of the samples is provided by square frames of scotch-"doubleface" on both sides of the spacer. When necessary, the samples are additionally sealed by Araldite (epoxy-glue).

The samples are studied using a polarizing microscope Leitz-Wetzlar with 10 X objective with a heating stage Mettler FP5. An automatic Pentax camera is used for texture pictures. During the heating to the L_α–I transition temperature (120–125°C) no substantial variations of the initial texture appears as noticed above. After the transition we get isotropic melt with some spherulites floating in it. Sometimes heating to 130°C is necessary to melt them entirely. Then we start to decrease the temperature very slowly (0.2°C/min) and after some undercooling (2°–4°C) below L_α–I transition the small spherulites appear again, but also a growth of a homeotropic monodomain

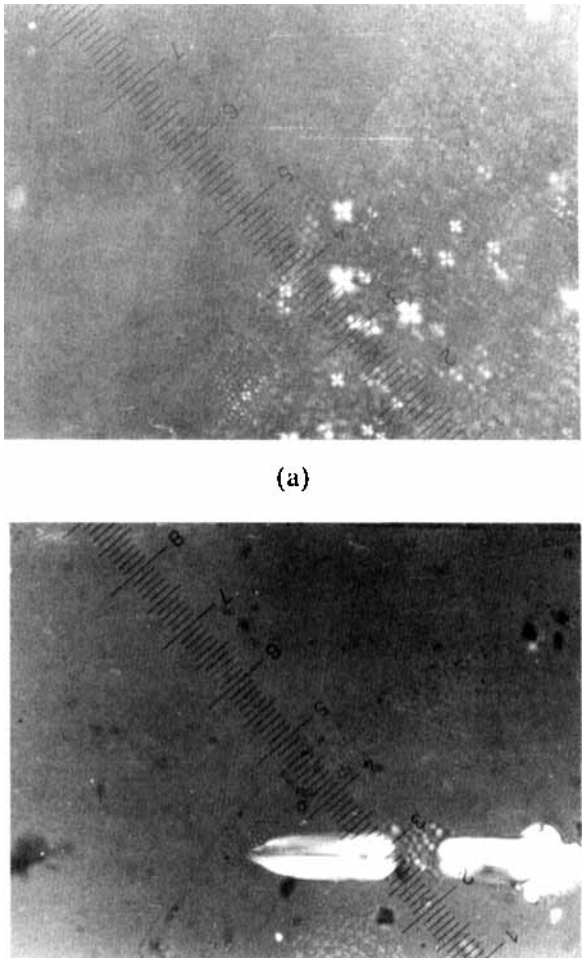

(a)

(b)

FIGURE 1 Growth of a homeotropic monodomain starting from the upper of the photo. The scale is 9 μm per line. (a) The spherulites are destroyed and get oriented at the border. (b) A batonnet is pushed in the isotropic melt, and disappears.

can be noticed, usually starting from the periphery of the drop (Figure 1a). This growth is assisted by the slow decrease of the temperature and after large undercooling (10–15°C) it spreads over the whole area of the drop. Small spherulites and some dust particles appear to be pushed by the front of the growing monodomain. Problems for the

monodomain growth come from the formation, in the isotropic melt, of batonnets (Figure 1b). They turn to be unable to penetrate by growing the homeotropic region, but if their density becomes substantial (the case of faster cooling), the growth of monodomains can be stopped. Sometimes we observe that by further slow cooling batonets can spontaneously disappear, but in other cases it is necessary to melt them by short thermal pulses (the batonets are thermally more labile than the formed monodomain, in which undulation instability is induced by these pulses, see below). Forming more easily at higher thicknesses, these batonets should eventually prevent the successful monodomain orientation at very large thickness. But all the studied samples up to 0.5 mm thickness were successfully oriented by this method. Finally, the central area of the drop becomes a perfect monodomain, and only at the drop periphery a rim of a length comparable to the sample thickness keeps a coloured disordered texture, probably because of aperipheral defects. Still, in the central part of the drop, a sufficient area for optical observations (0.25 cm^2 or more) remains homeotropic, hopefully with not strong change in initial EG concentration. The rim of coloured texture was not noticed to grow after a long incubation (several days) of the samples at 40–50°C.

At further cooling of the monodomain, edge dislocations are generated, sometimes decorated with small focal conics. They move along the monodomain area, evidently relaxing in this way the compressive strains due to the negative thermal expansivity of lecithin (see below). Their density could be increased by faster cooling.

X-RAY DETERMINATION OF THE REPEATING DISTANCE

This investigation is performed by a Laue camera (Philips) with CuK_α radiation (1.54 Å) and photographic registration. The mesophase is introduced in a 1.5 mm capillary by breaking the tip of the capillary and immersing it in the mesophase collected at the bottom of a Pyrex glass tube. By heating the mesophase to 130°C the viscosity of the melt is strongly reduced and a sufficient length is drawn up by the capillary forces. Then the tip and the bottom of the capillary is sealed by Araldite. After 12 h irradiation two fine Bragg reflections are observed at $2\theta = 0.036$ rad corresponding to a repeating distance of 43 Å, in a good agreement with Ref. 3. Assuming that EG and DLL have about the same density, we estimate the respective thicknesses of the EG and DLL layers to be 15 Å and 28 Å.

OBSERVATIONS OF THE UNDULATION INSTABILITY IN HOMEOTROPIC GEOMETRY

The undulation instability under a dilative stress is a well known phenomenon in thermotropic smectics A.[4,5,6] It was also observed in dipalmitoyl lecithin smectic A monodomains with very low water content,[2] giving a value of the penetration length $\lambda = \sqrt{K/B}$ (K-Frank elastic constant of splay, B-compression elastic constant along the layer normal) $\lambda \sim 100$ Å. In thermotropics with negative thermal expansion coefficients (long alkyl chain substituents) such instability was observed by pulses of heat.[7] This effect was briefly mentioned to exist in almost dry lecithin samples[2] and was further studied in aqueous and nonaqueous mesophases of lecithin in a planar geometry,[8,9] where it resulted in two sets of periodical striations, localized near to each glass boundaries of the planar monodomain. Indeed, the thermal expansion coefficient of egg lecithin is known to be negative, $\beta = -2.10^{-3}/°C$,[10] so by heating an array of parallel lipid bilayers confined in a fixed spacing, one can effectively put it under mechanical dilative stress.

In principle, there could be, in lyotropics, two regimes of such thermomechanical instabilities, at fast heating, when the solvent has no time to equilibrate in lateral direction and at slower heating, where it can. The relaxation mechanism involved here may be decomposed in hydrodynamic modes by Fourier analysis.[11] Their characteristic relaxation time is $\tau = \eta/Kq^2$ (η is a viscosity coefficient, K a Frank elastic constant, and q the wave-vector of the mode). The fondamental mode is the slowest one. Its half-wave length equals the width of the sample.

For a typical sample size L of a few millimeters, we calculate then that equilibrium is reached after several hours, much longer than the experimental time. So, in the following we restrict the discussion to the fast process. The effective thermal expansivity may then be expressed as

$$\beta_{\text{eff}} = \beta_{\text{DLL}} + \frac{\ell_{\text{EG}}}{\ell}\,\alpha_{\text{EG}} \simeq \beta_{\text{DLL}} + \frac{1}{3}\,\alpha_{\text{EG}},$$

where ℓ and ℓ_{EG} are the thicknesses of the total layer and of the EG layer, and where $\alpha_{\text{EG}} = 0.6375\ 10^{-3}/°C$ is the volume expansivity of the ethyl-glycol.

The threshold temperature increment can be obtained combining

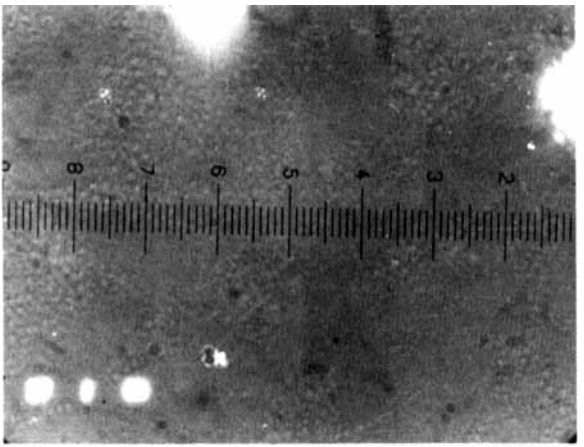

(a)

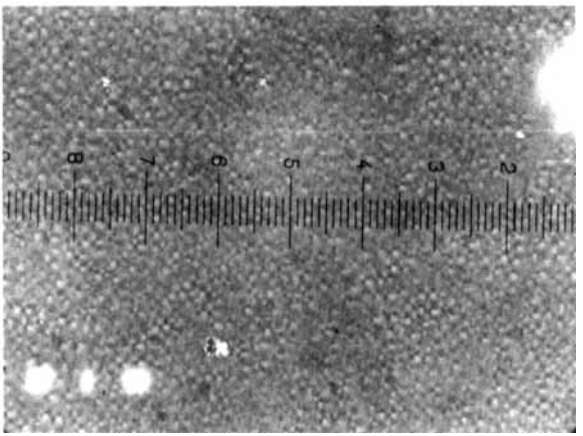

(b)

FIGURE 2 Thermal instability at ~50°C in a 410 μm thick sample, produced by a ΔT-jump. Same scale as in Figure 1. (a) ΔT = 0.5°C, just above threshold. The instability appears as isolated spots. (b) ΔT = 0.8°C. (c) ΔT = 1.2°C. (d) ΔT = 2°C. The grid is now transformed in a broken structure composed of focal conics. This structure keeps reversible, but cooling below the starting temperature is sometimes necessary to erase it.

$\delta_{th} = 2\pi\lambda^4$ for the threshold displacement and $\delta_{th} = -\beta_{eff}.d.\Delta T_{th}$, where d is the sample thickness:

$$\Delta T_{th} = \frac{2\pi\lambda}{|\beta_{eff}|d} \tag{1}$$

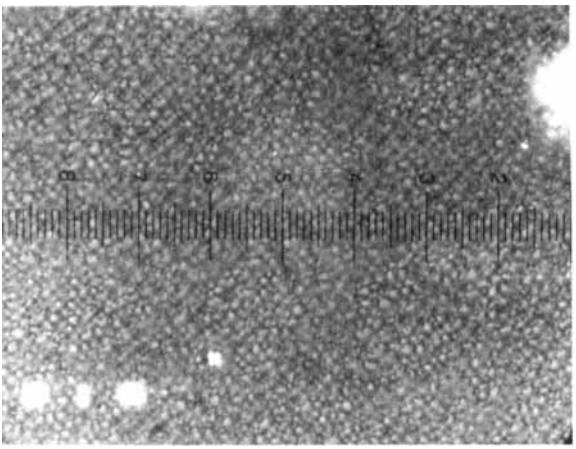

(c)

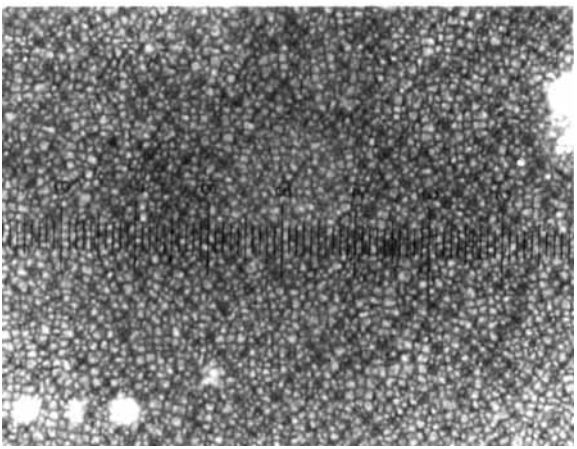

(d)

FIGURE 2 (con't.)

The wave vector of the instability q_c is expected to be[4]:

$$q_c = \sqrt{\frac{\pi}{\lambda d}} \tag{2}$$

Three sample thicknesses were studied: 100 μm, 250 μm, and 410 μm. As can be seen between crossed polarizers (Figure 2), the thermal instability makes a nearly square grid which is the superposition of

TABLE I

Thickness dependence of the threshold temperature increment for thermomechanical instability in DLL-EG lamellar phase (initial concentration of EG – 35% wt). The data refer to 68°C initial sample temperature, but no marked temperature dependence was noticed.

d [μm]	105 ± 5	250 ± 5	405 ± 5
ΔT_{th}[deg]	1.0 ± 0.2	0.6 ± 0.1	0.3 ± 0.1

two undulations of orthogonal q_c wave-vectors. The threshold determinations is not very accurate nor reproducible. Typical values are summarized in Table I. Near the threshold, the grid appears as a transient effect. Farther from the threshold, it is stable for a long time. It can however be erased by decreasing the temperature to the starting value, showing a complete reversibility. From these data, and Eq. (1), we can estimate $\lambda \sim 225 \pm 25$ Å. Typically, the half-period of the grid measured on the pictures is 10 ± 2 μm. From Eq. (2), we then deduce $\lambda \sim 200$ Å, in agreement with the estimation from the temperature threshold of the instability.

In fact, several points indicate that this measured value does not correspond to the true λ (which should be of the order of magnitude of the layer thickness, i.e. about 5 times smaller), because the measurement has not really been performed at the threshold of the instability. A first indication is that the undulation is never observed as a single grating of parallel stripes.[12] It appears also that the period of the instability as measured from the grid in the photos does not strongly depend on the sample thickness and that under this aspect, Eq. (2) is not strictly verified. Such an hypothesis of large excitation above threshold, is confirmed from light scattering measurements which, being more sensitive, allow to observe the real threshold of the thermal instability, and to measure the exact λ (~50 Å) (next section). It is also observed that the period of the instability increases when the threshold is overcome, which explains therefore the above finding of a too large λ value.

LIGHT SCATTERING STUDIES

For these studies the samples, after being observed under the polarizing microscope, are transferred to another oven with the same (or slightly lower) temperature in order to avoid undulation instabilities. The sample is illuminated by a laser beam of a 50 mW He–Ne laser

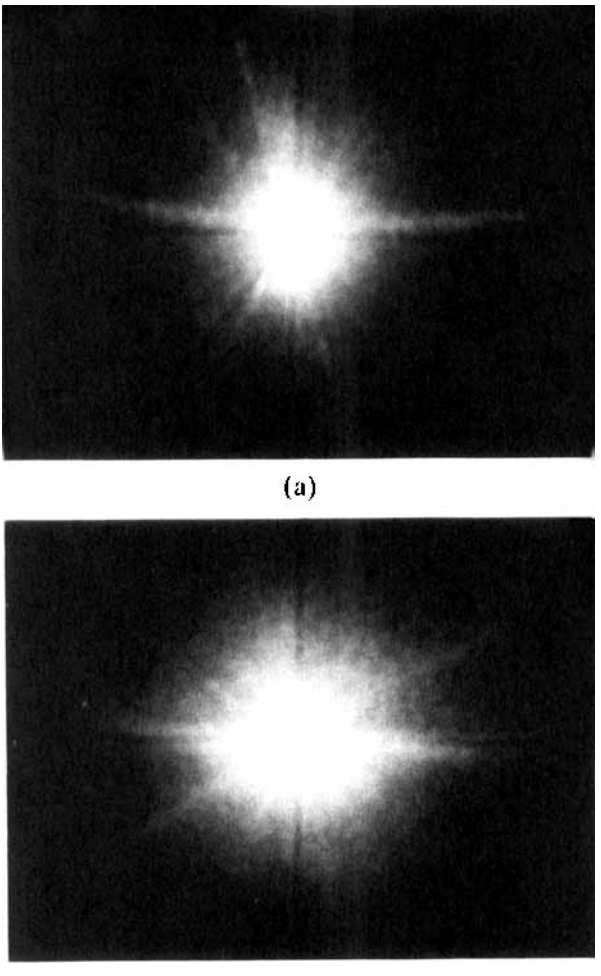

FIGURE 3 Typical crescent of light scattered (a) in the (e, o) configuration; (b) in the (o, e) configuration. The black cross points the direct beam. The light scattered from localized defects makes straight lines on the screen.

(Spectra-Physics) making a 45°-angle to the layers, in order to increase the coupling of the light with the expected layer undulation. In this way, it is possible to observe the undulation instability very near to the threshold. Similarly to what have been observed in thermotropics,[13] the instability produces a distortion of wave vector parallel to the layers, which scatters the light along a circle in both configurations: (o, e) (Figure 3), and (e, o), o and e standing for ordinary

and extraordinary polarization of the incoming and outcoming light. Just at threshold, the circle is irradied on the two symmetrical spots corresponding to q_c. We measure then $q_c \sim \frac{1}{4} q_o$, q_o being the wave vector of the light. We deduce $\lambda \sim 50$ Å which agrees more with the layer thickness than the previously determined 200 Å. At higher temperature jumps producing the already observed broken texture of Figure 2d (regular array of focal conics), the scattering becomes very diffuse within a cone around the laser beam, corresponding to a typical wave-vector smaller than q_c as mentioned in the previous section. From the distance of the laser beam to the circle on Figure 3 (which measures the smallest scattered wave-vector), and using Eq. 1 from Ref. 13, we deduce that the sample has a positive birefringence $\Delta n \sim 9 \times 10^{-3}$. This value is about 50 times smaller that the birefringence of the thermotropic liquid crystals. This explains that we failed to observe the quasielastic Rayleigh scattering of light by the thermally excited undulation mode. Data accumulations one thousand times longer than in thermotropic smectics A would have been necessary to give the same signal to noise ratio in this quasi elastic Rayleigh experiment. Note the difference with the swollen lamellar phases which have a complete lack of compression elasticity (B = 0), and which therefore exhibit a strong nematic like signal[14] from the dynamics of layer undulations.

MICROMECHANICAL MEASUREMENTS

We use a piezoelectric ceramics device, as described in Refs. 15–16, feeded by a.c. generator, in order to produce a variable displacement of one of the glass plates, cemented to a first piezoelectric ceramic. The stress transmitted to the second plate through the sample is detected by a second piezoelectric ceramic. The received signal is digitalized and accumulated in order to measure the stress amplitude and phase compared to the imposed displacement. The thickness between the glass plates is adjusted to 90 μm; the sample is then introduced in the isotropic phase at 130°C and oriented by slow cooling down to 36°C; the orientation is controlled under polarized optical microscope through the mechanical holder. The result is shown in Figure 4 where the mechanical impedance Z, ratio of the measured stress to the applied deformation, is plotted in the complex plane versus the frequency of the sinusoidal deformation.

We can observe that the response of the material is elastic for

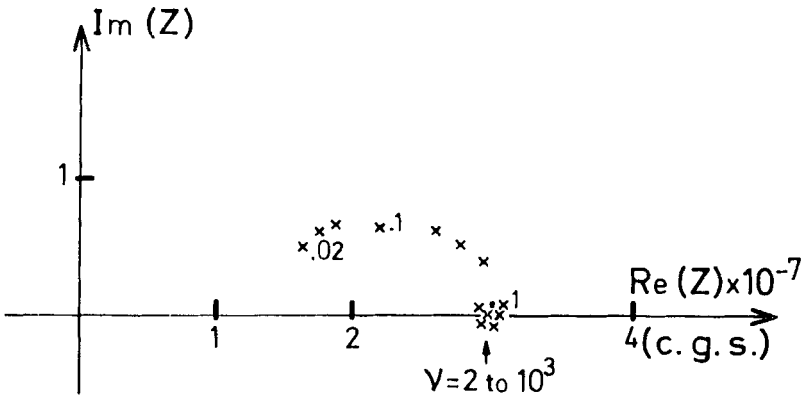

FIGURE 4 Mechanical impedance $Z = \sigma/\epsilon$ of DLL-EG under sinusoidal strain, plotted in the complex plane. The numbers near the points are frequencies.

frequencies between 1 and 5.000 Hz with a uniaxial compression elastic constant $B = 3\ 10^7$/cgs. At lower frequencies, from 1 to .02 Hz, a relaxation appears which may be due to movement of defects. The B value obtained in this experiment is lower than the one measured at 1 MHz in hydrated lecithin by flexoelectric excitation of the "second sound" resonance[17]: $B \sim 10^9$ cgs.

With the same device, we undertake to measure optically and mechanically the undulation threshold under a dilation normal to the layers. The applied deformation (either compressive or dilative) has a single square wave function form versus time, with a displacement amplitude between 8 and 1600 Å and a duration of 10 seconds. The signal received on the second ceramic is composed of an instantaneous elastic response, followed by an exponential relaxation, which corresponds to the low frequency dissipative part previously described. The stress σ_e, measured 5 ms after the starting step-function strain, is characteristic of the high frequency elastic response of the material. We have made successive deformations, increasing the voltage applied on the excitation ceramic, and keeping the sample at rest for 10 minutes for annealing between each measurement. We also observe the scattering of a laser light to control the undulation production at large dilative deformation.

Mechanical results are reported on Figure 5 which is a plot of σ_e versus the imposed displacements. For low dilative deformation, the measured stress σ_e is proportional to δ, but the slope of the curve $\sigma_e(\delta)$ becomes lower above a critical value δ_c which defines now the mechanical threshold; above δ_c, the decrease of slope corresponds to

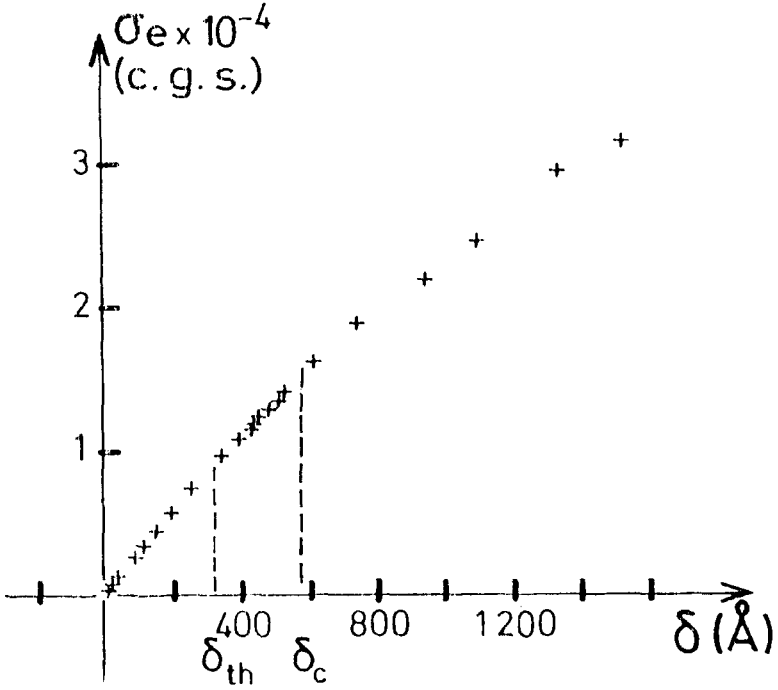

FIGURE 5 Stress σ_e versus displacement δ under square wave strain. Sample annealed between each measurement.

a lower dilation modulus. This effect does not appear under compressive strain, where no instability is expected. From the measured $\delta_c = 580$ Å, we deduce $\lambda = \delta_c/2\pi \sim 90$ Å, significantly larger than the value obtained from light scattering (50 Å).

To understand this discrepancy, we have reproduced the mechanical experiment without annealing. The excitation is now a continuous square wave, alternating compression and dilation every ten seconds. The instabilities which can appear during the dilation period, are stabilized during the next compressive period, so that a stationary state is reached. In that situation, the B elastic constant measured 5 ms after the beginning of each step, is found to be the same ($B \sim 3.10^7$ cgs). We find now (Figure 6) two critical displacements, one (δ_1) close to 400 Å, the other one (δ_2) at 1000 Å. This behavior can easily be explained. The lower threshold corresponds to that part of the sample without defects. The higher one, at 1000 Å, corresponds to the threshold of the region with high density of defects, which allow the layers to flow, increasing δ_c. The three straight lines ap-

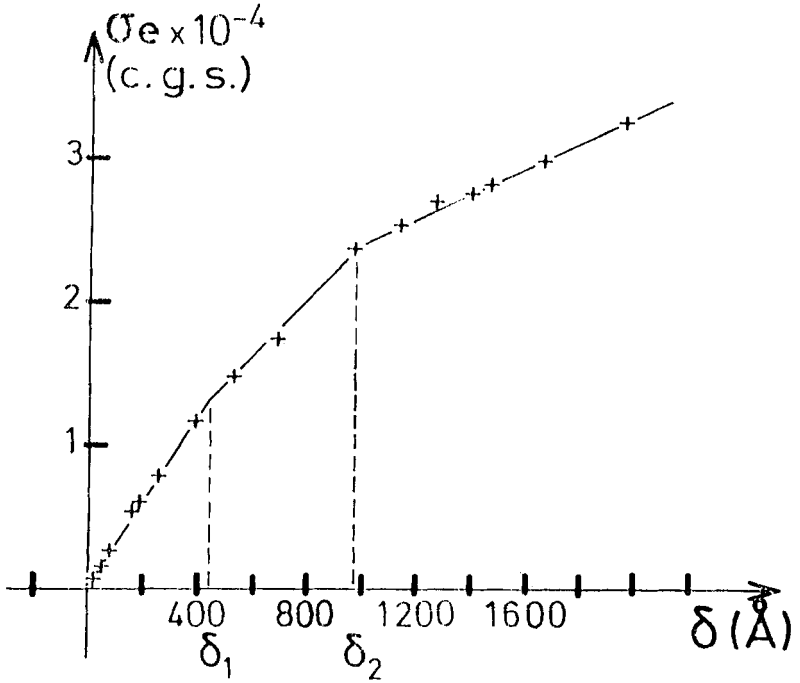

FIGURE 6 Same experiment as in Figure 5 without annealing between each measurement.

pearance of the $\sigma_e(\delta)$ curve is just due to the superposition of the signals from the two parts of the sample. From δ_1, we get a value of $\lambda \sim 70$Å, closer to the optical value (50 Å). We can now reanalyze the data from Figure 5. The value of 580 Å previously measured is much lower than $\delta_2 = 1000$ Å, because of the anneling, but corresponds obviously to the softer part of the sample. Looking more careful to the beginning of the $\sigma(\delta)$ curve of Figure 5 we can detect a small change of slope at $\delta_{th} = 330$ Å, which corresponds to $\lambda = 54$ Å. These last values of δ_{th} and λ are the best data which can be deduced from the mechanical measurement, and they compare indeed very well with the transient optical measurement of q_c, resulting in $\lambda = 50$ Å.

CONCLUSION

A new method for homeotropic monodomain formation of high solvent content lecithin-ethylenglykol lamellar lyomesophases by slow

crystallization of the isotropic melt between silane-treated glass plates is developed. Thermomechanical undulation instabilities are observed in these monodomains, starting always as a rectangular grid. Mechanical experiments, microscopic and light scattering studies of this instability allow the estimation of some material constants of this lamellar phase. The compression elastic constant in a direction normal to the layer is $B = 3\ 10^7$ cgs at T = 40°C. All the measurements of the threshold instability and the undulation wave length are consistent and correspond with a penetration length $\lambda = 50$ Å. From this value we deduce the Frank elastic constant of splay $K = B\lambda^2 = 7.5\ 10^{-6}$ dyne. Thus, using $d = 43$ Å for the repeating distance, the curvature modulus of a single bilayer may be evaluated to $K_c = Kd = 3.2\ 10^{-12}$ erg in good agreement with the value obtained by Helfrich and al.[18]

The dilauroyl-lecithin-ethylenglycol system is a good example of a smectic A like liquid crystal at room temperature and below (the hydrated DLL has a gel liquid crystal transition at 0°C) with remarkably broad range of thermal stability (above 100°C). This allows for a temperature variation of its viscosity in broad limits. The method of homeotropic domain growth and the undulation instability in such domains could be useful in the construction of molecular electronics devices.

Acknowledgments

One of the authors (A.G.P.) is indebted to L. Liébert, J. Charvolin, A. M. Levelut, R. Ribotta, J. Prost and J. P. Marcerou for very helpful discussions and to J. L. Rank for a gift of DLL and EG; he acknowledges the financial support from CNRS and Bulg. Acad. Sci. making possible this investigation in the frame work of the cooperation on the theme "Molecular Fluids" between CNRS and BAS.

References

1. N. Moucharafich and S. Friberg, *Mol. Cryst. Liq. Cryst.*, **49**, 231 (1979).
2. L. Powers and N. A. Clark, *Proc. Nat. Acad. Sci. USA*, **72**, 840 (1975).
3. M. A. El-Nokaly, L. D. Ford, S. E. Friberg and D. W. Larsen, *J. Coll. Interface Sci.*, **84**, 228 (1981).
4. M. Delaye, R. Ribotta and G. Durand, *Phys. Letters*, **44A**, 139 (1973).
5. N. A. Clark and R. B. Meyer, *Appl. Phys. Lett.*, **22**, 493 (1973).
6. R. Ribotta and G. Durand, *J. Physique*, **38**, 179 (1977).
7. R. Ribotta, *J. Physique Coll.*, **37**, C3-149 (1976).
8. A. G. Petrov and G. Durand, *J. Physique-Lett.*, **44**, 793 (1983).
9. A. G. Petrov, S. Chumakova and S. Naydenova, *Kristallografiya*, **29**, 1138 (1984).
10. R. P. Rand and W. A. Pangborn, *Biochim. Biophys. Acta*, **318**, 299 (1973).

11. R. Bartolino and G. Durand, *J. Phys.*, **42**, 1945 (1981).
12. J. M. Delrieu, *J. Chem. Phys.*, **60**, 1081 (1974).
13. R. Ribotta, G. Durand and J. D. Litster, *Sol. State Comm.*, **12**, 27 (1973).
14. J. M. Meglio, M. Dvolaitzky, L. Leger and C. Taupin, *Phys. Rev. Lett.*, **54**, 1686 (1985).
15. M. Cagnon and G. Durand, *Phys. Rev. Lett.*, **45**, 1418 (1980).
16. M. Cagnon, J. F. Palierne and G. Durand, 18ème Coll. Ann. du groupe français de Rhéologie (1983).
17. J. P. Marcerou, J. C. Rouillon and J. Prost, *Mol. Cryst. Liq. Cryst.*, **102**, 211 (1984).
18. G. Beblik, R. M. Servuss and W. Helfrich, *J. Physique*, **46**, 1773 (1985).